A new statistical approach to improve the satellite based estimation of the radiative forcing by aerosol- cloud interactions

Piyushkumar N Patel[1], Johannes Quaas[2], Raj Kumar[1]

[1]Space Applications Centre, ISRO, Ahmedabad, India
[2]Institute for Meteorology, Universität Leipzig, Leipzig, Germany

Corresponding to: Piyushkumar N Patel (piyushether@gmail.com)

Abstract

In a previous, study of *Quaas et al., (2008)* the radiative forcing by anthropogenic aerosol due to aerosol-cloud interactions, RF_{aci}, was obtained by a statistical analysis of satellite retrievals using a multilinear regression. Here we employ a new statistical approach to obtain the fitting parameters, determined using a non-linear least square statistical approach, for the relationship between planetary albedo and cloud properties and, further, the relationship between cloud properties and aerosol optical depth. In order to verify the performance, the results from both statistical approaches (previous and present) were compared to the results from radiative transfer simulations over three regions for different seasons. We find that the results of the new statistical approach agree well with the simulated results both over land and ocean. The new statistical approach increases the correlation by 21%-23% and reduce the error, compared to the previous approach.

1 Introduction

Aerosols are considered to have a large effect on climate, both through aerosol radiation interactions, and through aerosol-cloud interactions by serving as cloud condensation nuclei (CCN), therefore increasing N_d and thus cloud albedo (*Twomey, 1974*), as well as rapid cloud adjustments (*Boucher et al., 2013*). Much work has been done to quantify the radiative forcing by aerosol-cloud interaction (RF_{aci}), yet it remains highly uncertain. The annual radiative forcing from aerosol induced changes in cloud albedo were reported as -0.7 Wm^{-2} with an uncertainty range -1.8 to -0.3 Wm^{-2} (*Boucher et al., 2013*); this effect could offset much of the warming from greenhouse gases (*Huber and Knutti, 2011*), emphasizing the need to understand the effect so that we can better predict the future climate.

In this study, we concentrate on the RF_{aci}, the change in cloud albedo with increasing aerosol. An increasing aerosol at constant cloud water content is supposed to decrease droplet size, which in turn increases the cloud albedo due to the increase scattering of the smaller, more numerous cloud droplets. *Feingold et al. (2001, 2003); McComiskey et al., (2009)* proposed a metric to quantify the microphysical component of the cloud albedo effect ($ACI = -d \ln N_d / d \ln \alpha$), where N_d is the cloud droplet number concentration and α in some proxy for the aerosol burden. A variety of proxies has been used to represent the cloud response to the change in aerosol, e, g., cloud optical depth (τ_c), cloud drop number concentration (N_d) and cloud droplet effective radius (r_e). Similarly, various proxies have been used to represent the total ambient aerosol burden, including aerosol number concentration (N_a), aerosol optical depth (τ_a) and aerosol index (AI). An overview about published relationships and their biases

due to mismatches between process- and analysis scales are discussed in *McComiskey and Feingold, (2012)*. Values for ACI metrics from observations often differ significantly from model-based values (*Quaas et al., 2008, 2009; Bellouin et al., 2008; Penner et al., 2011, 2012*). For example, the observational-based values of RF_{aci}, often in the range of -0.2 to -0.6 Wm^{-2} (*Quaas et al., 2008; Bellouin et al.,2013*), is tend to be weaker than the modeled values in the range of -0.5 to -1.9 Wm^{-2} (*IPCC, 2007*). The differences in model and observational-based RF_{aci} have to be reconciled. *Penner et al., (2011)* reported that the lower sensitivities of cloud droplet number concentration, when considering aerosol optical depth (AOD) compared to aerosol index as aerosol quantity may lead to a significant underestimation in satellite-based RF_{aci}. However, *Quaas et al., (2011)* pointed out the weaknesses in the approach used by *Penner et al., (2011)*. Clearly, further study is needed to reduce the uncertainties in both observational- and model-based estimates of aerosol RFaci and to reconcile the differences.

Quaas et al., (2008) derived the anthropogenic aerosol RF_{aci} based on satellite retrievals of aerosol and clouds properties using statistical relationships between cloud properties and anthropogenic aerosols without the use of radiative transfer model. They developed a statistical relationship between planetary albedo and cloud properties using a multilinear fit, and further, the relationships of cloud properties and aerosol optical depth. *Quaas et al. (2008)* suggested that uncertainties in the statistical relationship and fitting parameters introduced uncertainty in the estimate of RF_{aci}. Therefore, it is useful to reassess the estimated RF_{aci} by using a new statistical fitting approach. The main objective of this study is to explore the uncertainty in the satellite-based quantification of RF_{aci}. This study differs from previous studies by introducing new statistical fitting approach to obtain the fitting parameters for the estimates of RF_{aci}, determined using a nonlinear fit between planetary albedo and cloud properties. To verify the present approach, the results from both statistical approaches are compared with the results from a radiative transfer model.

The rapid socio-economic development in the recent past has increased the anthropogenic emissions in the South asian region along with several parts of the world. The South Asian ones are among the potential sources of a variety of aerosol species; both natural and anthropogenic, and extensive investigations are being made in the past years (e.g., *Chin et al., 2000; Di Girolamo et al., 2004; Moorthy et al., 2013*). These densely populated regions with the increasing power demand, fuel consumption and equally diverse geographical features are also vulnerable to the impacts of atmospheric aerosols to the climate (e.g. *Liu et al., 2009*). The complex geography of this region contributes significant amounts of natural aerosols (desert dust, pollen, sea-salt etc) into the atmosphere, which mix with anthropogenic ones, making the aerosol environment one of the most complex in the world (*Moorthy et al., 2015*). The large spatial heterogeneity of the sources coupled with the atmospheric dynamics driven by topography and contrasting monsoons, make South Asia's aerosol very difficult to characterize and to model their implications on radiative and climate forcing. While tropospheric perturbations would produce strong regional signatures, their global impacts still remain marginally above the uncertainty levels (*IPCC, 2013*). In the recent years, several studies are carried out on the aerosol characterization and its direct effect over south Asia, but there have been very few studies reported on the aerosol indirect effect using ground- and satellite-based measurements due to complex aerosol and cloud environments. Therefore, we discuss the RF_{aci} for both anthropogenic and natural fraction of aerosol for a period of six-years (2008-2013) for three different regions of south Asia (**Fig. 1**, Arabian Sea (AS; 63°E-72°E, 7°N-19°N), Bay of Bengal (BOB; 85°E-94°E, 7°N-19°N) and Central India (CI; 75°E-84°E, 20°N-30°N)), having

significantly distinct aerosol environments as a result of variations in aerosol sources and transport pathways (*Cherian et al., 2013; Das et al., 2015; Tiwari et al., 2015*). Additionally, we also discuss the uncertainties of the results in the following sections.

2 Data

We combine measurements of aerosol, cloud and radiative properties to derive the top-of-the atmosphere (TOA) RF_{aci} for both anthropogenic and natural aerosols. Data acquired by MODerate Resolution Imaging Spectroradiometer (MODIS) and Clouds and the Earth's Radiant Energy System (CERES) mounted on Aqua (*Parkinson, 2003*) and Ozone Monitoring Instrument (OMI) onboard Aura (*Schoeberl et al., 2006*) are used in this study. We use the broadband shortwave planetary albedo (α) (*Wielicki et al., 1996; Loeb, 2004; Loeb et al., 2007*) as retrieved by the CERES in combination with cloud properties from the MODIS (*Minnis et al., 2003*) and AOD (τ_a) and fine mode fraction (FMF) as retrieved by the MODIS onboard Aqua (*Remer et al., 2005*). Albedo and cloud properties are from the CERES Single-Scanner-Footprint (SSF) Level-2 Edition-3A data set at 20×20 km^2 horizontal resolution and aerosol properties (AOD and FMF) at 550nm from the MYD04 level-2 collection-5.1 dataset at 10×10 km^2 horizontal resolution are used. We used UV-aerosol index (UV-AI; *Torres et al., 1998*) measured by OMI-AURA (*Levelt et al., 2006*) from the OMAERUVG level-2 version 003 dataset at 0.25°×0.25° grid, which is a gridded dataset containing retrievals from the OMAERUV (*Torres et al., 2007*) algorithm. The data from CERES and MODIS level-2 products are interpolated to a 0.25°×0.25° regular longitude-latitude grid to separate the aerosol and cloud properties for anthropogenic and natural aerosols using UV-AI. Daily data, taken at roughly 13:30 local time, cover the 2008-2013 period.

3 Methods

All statistics between aerosol and cloud properties are computed separately for 3 regions and for each month of data at 0.25°×0.25° grid resolution. To avoid the greater uncertainty that exists in a clear distinction between aerosols and clouds and accurate retrieval of cloud properties, only single-layer cloud with liquid water path (LWP) > 20 gm^{-2} are taken into account. RF_{aci} for anthropogenic and natural aerosols are calculated using the methods outlined by *Quaas et al., (2008)* with the new statistical approach. As a part of this process, the method by *Kim et al., (2007)* MODIS-OMI algorithm (MOA) is employed to classify the aerosol types into one of four types sea-salt, carbonaceous, dust and sulfate using MODIS FMF and OMI UV-AI data. FMF provides information on the representative size of the aerosol. FMF is close to 1 for mostly small aerosol particles, which implies an anthropogenic origin and FMF becomes small for non-anthropogenic aerosol like dust. UV-AI allows to detect the absorption due to the presence of an aerosol layer by utilizing the sensitivity of absorptive aerosol in UV. Under most condition, UV-AI is positive for absorbing aerosols and negative for non-absorbing aerosols. Using these two independent data sets, aerosol can be classified. Details for the aerosol classification are discussed in *Kim et al., (2007)*. For the purpose of this research, the combination of dust and sea-salt AOD considered as a natural AOD and an anthropogenic AOD contains the combination of carbonaceous and sulfate. Further, the RF_{aci} is estimated for both anthropogenic and natural aerosols.

3.1 Satellite-based estimate of RF_{aci}

RF_{aci} is a function of the relationship between AOD and N_d in a cloud. N_d is not directly provided by satellite product and must be computed using cloud optical thickness (τ_c) and

effective droplet radius (r_e) for liquid water clouds assuming adiabaticity (*Brenguier et al., 2000; Schüller et al., 2005; Quaas et al., 2006; Bennartz, 2007; Rausch et al., 2010*).

$$N_d = \gamma \tau_c^{1/2} r_e^{-5/2} \quad (1)$$

Where, a constant value of $\gamma=1.37\times10^{-5}$ $m^{-0.5}$ (*Quaas et al., 2006*) is used in this study. A limitation of this assumption is that it applies rather well for the stratiform clouds in the marine boundary layer, but less so for convective clouds. A detailed explanation and uncertainty assessment are described in *Bennartz, (2007) and Rausch et al., (2010)*. Recently, *Bennartz and Rausch, (2017)* show that the uncertainties in the CDNC climatology from 13-years of AQUA-MODIS observations are in the order of 30% in the stratocumulus regions and 60% to 80% elsewhere and its contribution to the total uncertainty for this study is discussed in the following section.

Quaas et al., (2008) have adopted the *Loeb (2004)* approach for the estimate of planetary albedo. Albedo (α) of a cloud scene can be well described by a sigmoidal fit as

$$\alpha \approx (1-f)[a_1 + a_2 ln\tau_a] + f[a_3 + a_4(f\tau_c)^{a_5}]^{a_6} \quad (2)$$

Where, α_1- α_6 are fitting parameters obtained by a multilinear regression, where α_5 is set as 1 (*Ma et al., 2014*). Dependency of τ_a is introduced to include the clear part of the scene in the above equation and f is the cloud fraction. The satellite-based estimate of RF_{aci} for anthropogenic and natural aerosols can be expressed as

$$\Delta F_{ant/nat}^{RF_{aci}} = f_{liq}.A(f,\tau_c)\frac{1}{3}\frac{d\ln N_d}{d\ln \tau_a}\left[\ln \tau_a - \ln(\tau_a - \tau_a^{ant/nat})\right] S \quad (3)$$

$$where, A(f,\tau_c) = a_4 a_5 a_6 \left[a_3 + a_4(f\tau_c)^{a_5}\right]^{a_6-1}(f\tau_c)^{a_5}$$

$d \ln N_d / d \ln \tau_a$ is the sensitivity of cloud droplet number concentration (N_d) to a relative change in AOD. It is computed as the slope of the linear regression fit between the natural logarithm of N_d and AOD (*Quaas et al., 2008*). This value is calculated on a month-by-month basis and is unique to each region studied. τ_a is the total AOD, whereas, $\tau_a^{ant/nat}$ are the anthropogenic and natural AOD, respectively, derived from the FMF and UV-AI as estimated above. A(f, τ_c) is the empirical function relating albedo to f and τ_c. S is the daily mean solar incoming solar radiation. RF_{aci} is calculated separately for the anthropogenic and natural aerosols for all three regions for each month.

A goal of the present study is to assess the uncertainty in the satellite-based estimate of the RF_{aci}. For that purpose, we adopted the new statistical nonlinear least square fitting approach to obtain the six fitting parameters in Eq. (2). Nonlinear least square methods involve an iterative improvement to parameters values in order to minimize the residual sum of squares between the observed values and the predicated value of the dependent variables. We used the Levenberg-Marquardt (L-M) algorithm (*Levenberg, 1944*) in the nonlinear least square approach to adjust the parameter values in the iterative procedure. This algorithm combines the Gauss-Newton method and the gradient descent method. In the gradient descent method, the sum of the squared errors is reduced by updating the parameters in the steepest descent direction. In the Gauss -Newton method, the sum of the squared errors is reduced by assuming the least squares function is locally quadratic, and finding the minimum of the quadratic. The L-M algorithm acts more like a gradient descent method when the parameters are far from the optimal value and acts more like to Gauss-Newton method when the parameters are close to their optimal value. More detail of this method is given in the literature (*Levenberg, 1944;*

Transtrum et al., 2010; Transtrum and Sethna, 2012). In the present study, instead of considering α_5=1 in the multiple regression, as in *Quaas et al. (2008) and Ma et al., (2014),* we obtained the values of all six fitting parameters using a nonlinear fitting approach (L-M algorithm) for each month and region. To get an impression of the performance of our statistical approach, we correlate α and RF_{aci} at TOA obtained from both statistical fitting methods (multilinear and nonlinear) vs. α and RF_{aci} simulated by radiative transfer model for all three regions. The following section describes the detail information about the simulation of α and RF_{aci} using the radiative transfer model.

3.2 Simulation of planetary albedo (α) and RF_{aci}

In order to verify both the statistical approaches, we performed a radiative transfer simulation to obtain α and RF_{aci} for all three regions. Radiative transfer calculations are performed with the SBDART [Santa Barbara DISORT Atmospheric Radiative Transfer; *Ricchiazzi et al., 1998*] that is a plane-parallel radiative transfer code based on the DISORT algorithm for discrete-ordinate-method radiative transfer in multiple scattering and emitting layered media (*Stamnes et al., 1988*). The discrete ordinate method provides a numerically stable algorithm to solve the equations of plane-parallel radiative transfer in a vertically inhomogeneous atmosphere. Simulations are carried out for the solar spectrum (0.2-4.0μm) for all three regions. Following the study by *Quaas et al., (2008)* study, *Bellouin et al., (2013)* performed a similar study with MACC reanalysis data, in which RT simulations, using a Monte -Carlo method, were carried out to obtain the standard deviation for the uncertainty analysis. However, in the present study, RF_{aci} is simulated using an RT model (SBDART) to validate the performance of both the statistical approaches used to compute the RF_{aci} using the statistical relationship between satellite measurements.

In the present study, simulations are carried out to simulate first α and later RF_{aci} for the given inputs. Here α is evaluated as the ratio of broadband outgoing (or upwelling) shortwave flux to the incoming (or downwelling) solar flux. Inputs to the model include profiles of temperature and water vapor which are resolved into 32 layers extending from 1000 to 1 mbar and come from European Centre for Medium-range Weather Forecast (ECMWF) reanalysis data. **Table 1** shows the list of input parameters and their source provided to the RT model for the estimate of RF_{aci}. Total columnar amount of atmospheric ozone is provided from OMI-AURA. Surface albedo is set to 0.15 to represent a typical land cover value for CI and, predefined option of the ocean surface is used for the oceanic regions (AS and BOB). In the SBDART model, the cloud parameter inputs are effective droplet radius (r_e), liquid water path (LWP) and the cloud fraction, all of which are taken from MODIS retrievals reported in the CERES-SSF product. The geometrical thickness of cloud (CGT) is computed as a difference between cloud top and bottom heights. Cloud top height is taken from CERES-SSF product and cloud base height is evaluated using the geopotential height profile from ECMWF data. Only liquid water clouds are considered in the estimation of RF_{aci}. The upwelling and downwelling fluxes are computed individually computed for all three regions at satellite (MODIS-Aqua as a reference) overpass time.

The local radiative forcing associated with the RF_{aci} is estimated as the difference between the perturbed and unperturbed radiative fluxes caused by perturbation in N_d due to the addition of aerosols while keeping the same meteorology. RF_{aci} is diagnosed by making two calls to the radiative transfer code: the first call used the unperturbed satellite-derived N_d and the second used perturbed N_d due to anthropogenic and natural aerosols. The numerical evaluation of

radiative flux for the perturbed case starts by determining the finite perturbation of cloud droplet number concentration (ΔN_d), calculated as follows:

$$\Delta N_d^{ant/nat} = \frac{d \ln N_d}{d \ln \tau_a} [\ln \tau_a - \ln(\tau_a - \tau_a^{ant/nat})] \quad (4)$$

The finite perturbation in N_d are evaluated separately for anthropogenic and natural aerosol to estimate the radiative flux for the perturbed case. The perturbed value of N_d' ($N_d + \Delta N_d$) is used to obtain a perturbed value of r_e using Eq. (5) for constant liquid water content because r_e is used as an input to the radiative transfer code.

$$N_d' = q_l / (\frac{4}{3} \pi {r_e}^3 \rho_w) \quad (5)$$

Where, ρ_w is the liquid water density, q_l the liquid water content (q_l=liquid water path / geometrical thickness). RF_{aci} is diagnosed as $RF_{unperturbed}$ - $RF_{perturbed}$ radiative fluxes at the top of the atmosphere, because increased concentrations of aerosol reduce the effective radius of cloud particles and smaller cloud particles reflect more radiation back to space. The following section describes the details of regression analysis of α and RF_{aci} performed between values from statistical-approaches and simulated values.

4 Results

4.1 Regression analysis

As stated in section 3.1, the satellite-based estimates of RF_{aci} are dependent on the fitting parameters α_1-α_6, obtained here from the two different statistical fitting approaches (multilinear and nonlinear). The parameters obtained from these two approaches are listed in **Table S1** for all three regions investigated in this study. These parameters vary with months since we conducted both the fitting approaches for each month, but only the mean seasonal parameters are shown here. The main differences in fitting parameters from both methods are found in the values of α_4, α_5 and α_6. The magnitude of the coefficients α_4 and α_6 is larger in the nonlinear fit than the multilinear regression fitting, which may reduce the magnitude of the coefficient α_5. To accomplish the objective of this study, we correlate α and RF_{aci} at TOA obtained from both statistical fitting approaches (multilinear and nonlinear) with estimates obtained from radiative transfer model for all three regions. **Fig. 2** shows scatter density plots of comparison between model-simulated albedo and the one computed from satellite measurements at 0.25°×0.25° grid resolution using both statistical methods for all three regions. This regression analysis suggests that the albedo fitted by the new statistical approach (nonlinear fit) agrees well with the model-simulated albedo over both land and ocean. The scatter of the results from the nonlinear fit around the 1:1 line is much smaller compared to multilinear fit, which is also reflected in the coefficients of determination (R^2) ranging from 0.74 to 0.79. However, a reduction in over and underestimation at very large and very small albedos, respectively, is found in the nonlinear fit compared to the multilinear statistical approach. This is also clearly reflected in the values for the root mean square error (RMSE), which reduces from 0.042-0.065 to 0.010-0.017, supporting the expectation that the new statistical method is more reliable. Additionally, a comparison between the planetary albedo computed using both statistical fits and the CERES retrieved albedo is shown in **Fig. S1** for all three regions. Similar to the results discussed above, the analysis shows a good agreement between the CERES derived albedo and the one calculated using the nonlinear fit.

In addition, we performed a comparison of RF_{aci} obtained from satellite measurements using both statistical approaches with the one simulated by SBDART for each season and for each region. **Fig. 3** illustrates the linear regression of RF_{aci} from the two statistical approaches plotted against the one obtained from the radiative transfer model for both anthropogenic and natural aerosols for all seasons and all three regions. The analysis showed good statistical agreement with Pearson's correlation coefficient r=0.82 and 0.75 and RMSE=0.037 Wm^{-2} and 0.042 Wm^{-2} for the anthropogenic and natural fraction of aerosols, respectively. An examination of **Fig. 3** reveals that the nonlinear fitting approach reduces the scatter seen for the multilinear fit and the improvement in correlation with the simulated forcing. The nonlinear fit increases the correlation by 21%-23% and reduce the RMSE by 0.007-0.011 W m^{-2} compared to the multilinear approach. The relative difference between the RT-simulated and the statistically computed RF_{aci} are computed for both the statistical methods. The mean relative difference in RF_{aci} for anthropogenic fraction of AOD is 0.021 W m^{-2} in the nonlinear and 0.033 W m^{-2} in the multilinear statistical approach, whereas, for RF_{aci} of natural fraction of AOD, it is 0.032 W m^{-2} in nonlinear and 0.053 W m^{-2} in multilinear statistical approach. This suggests that the use of the nonlinear fitting approach reduces the uncertainty by 36%-39% compared to the multilinear regression.

4.2 RF_{aci} and Uncertainties

Aerosols and clouds vary substantially as a function of time in all regions; thus it is interesting to analyses aerosol-cloud interactions as a function of season. **Fig. 4** shows the seasonal variability of six-year averaged radiative forcing by aerosol-cloud interaction for the three regions as defined above. The maximum anthropogenic RF_{aci} is found over oceanic regions (AS: -0.15Wm^{-2}, BOB: -0.16Wm^{-2}), instead of regions over land (CI: -0.12 Wm^{-2}) with high anthropogenic emissions. This is because maritime clouds are more susceptible to changes in concentration of anthropogenic aerosols (*Quaas et al., 2008*). In contrast, the natural RF_{aci} is generally stronger over land (-0.15 Wm^{-2}) than over oceanic regions (AS: -0.098 Wm^{-2}, BOB: -0.07Wm^{-2}). It is seen that the anthropogenic RF_{aci} is strongest during winter over AS and BOB, with values near -0.19 Wm^{-2} and -0.22Wm^{-2}, whereas it is strong (-0.2 Wm^{-2}) during pre-monsoon over CI (land). The dominance of natural aerosols in pre-monsoon results a large natural RF_{aci} both over land (-0.15 Wm^{-2}) and ocean (-0.098 Wm^{-2} and -0.07 Wm^{-2}).

A direct comparison of the satellite to simulations-based RF_{aci}, shows a good correlation. However, both satellite estimated and simulated RF_{aci} are subject to errors and it is useful to compute the associated uncertainties in the above results due to various parameters. Uncertainty involves the ones due to satellite retrievals of AOD which can be highly biased in the vicinity of cloud due to swelling (*Koren et al., 2007*), and also due to 3D effects (*Wen et al., 2007*). Since both biases may be particularly high for thick clouds, our estimate of the RF_{aci} could be still be overestimated. The uncertainty in MODIS retrievals of AOD from validation studies (*Levy et al., 2007*) was quantified at $0.03+0.05\tau_a$ over ocean and $0.05+0.15\tau_a$ over land. However, since we use the MODIS-OMI algorithm (*Kim et al., 2007*) to estimate the anthropogenic and natural fraction of AOD, uncertainty in this is given as 1σ standard deviations as per Table S2. From satellite intercomparison, the uncertainty in radiative flux retrievals by CERES is estimated at 5% (*Loeb, 2004*), and uncertainty in cloud optical depth is 21% (*Minnis et al., 2004*). The uncertainties due to sensitivity of N_d to a relative change in AOD ($d \ln N_d / d \ln \tau_a$) contribute most to the total uncertainty. For N_d sensitivities to changes in AOD, standard deviations are derived from minimum and maximum values obtained for

each season. Following the study by *Bellouin et al., (2013)*, the standard deviations are derived from minimum and maximum values by defining 4-sigma interval, which covers the large range of sensitivities and spatio-temporal variabilities. To define the standard deviations in RF_{aci} due to variation in $d \ln N_d / d \ln \tau_a$, RF_{aci} is recomputed using those standard deviations of N_d sensitivities to changes in AOD. Table 2 shows the seasonal and regional sensitivities of $d \ln N_d / d \ln \tau_a$ along with their statistical standard deviation, which is computed from the minimum and maximum values for each season. The associated range in RF_{aci} both for anthropogenic and natural fraction of AOD is also shown in Table 2, where the standard deviation of RF_{aci} shows the variation due to change in $d \ln N_d / d \ln \tau_a$, which finally contribute to the total uncertainty. In addition to this, the computed RF_{aci} in this study is associated with the statistical fitting approach as described in section 3. As mentioned earlier, two different statistical fitting methods are used to obtain the regression coefficients for the estimate of RF_{aci}. In the present study, except for the statistical fitting method, all the variables and methodologies are same for both the statistical approach. Therefore, we used the relative difference between the RT-simulated and statistically computed RF_{aci} as an uncertainty due to the choice of the statistical fitting approach for both the statistical fitting methods. As shown in section 4.1, the mean relative differences for the nonlinear and multilinear approaches are 0.021 W m^{-2} and 0.033 W m^{-2}, respectively, in RF_{aci} for anthropogenic fraction, whereas, for the RF_{aci} of the natural fraction of AOD, these are 0.032 W m^{-2} and 0.053 W m^{-2} for nonlinear multilinear statistical approaches, respectively. Table 3 lists the uncertainty due to different parameters involved in the satellite-based estimate of RF_{aci}. We quantify the relative error as the square root of the sum of the squared relative errors for all individual contributions. This yields an influence of these relative uncertainties in the input quantities on the computed RF_{aci} of ~±0.08Wm^{-2}. It should be noted that we refer here to the published quantifiable uncertainties in the satellite retrievals. Limitation involved in this approach or uncertainties in the satellite retrievals contribute to the overall uncertainty, which is difficult to quantify.

In addition to above error budget, there are uncertainties involved in the RT simulated RF_{aci} due to various parameters as shown above. In this regard, the surface albedo plays a major role in the simulation of RF_{aci}. In the standard approach, we have considered a surface albedo value 0.15 for land and the predefined option for the ocean surface albedo is used for the oceanic regions in the present study. To quantify the uncertainties involved due to assumptions about the surface albedo, we have simulated RF_{aci} with different plausible surface albedo values and computed statistics as shown in **Table S3(a) and S3(b)**. The statistics shows that the considered values of surface albedo are suitably representative of the study regions. In addition, RT simulation have their own limitations and uncertainties e.g. inherent code accuracy, overestimate in calculated RF due to plane-parallel bias, 3-D radiative transfer effect etc. It would be useful to explore these issues in the future. However, in the present study, RT simulation is used to evaluate the results computed with satellite- based measurements. There is a scope to improve the present study with the upcoming data set retrieved from spaceborne active remote sensing instruments, with the improved satellite products and with the new statistical relationship.

5 Conclusions

In this study, we employed a new nonlinear statistical fitting approach to develop the statistical relationship. A satellite-based algorithm is used to quantify the anthropogenic and natural fraction of aerosol optical depth for the computation of RF_{aci} from satellite retrievals. In order to verify, α and RF_{aci} estimates using the new statistical approach (nonlinear) along

with the previous statistical approach (multilinear fit), these are compared with the results obtained from radiative transfer simulations. The results show a better agreement between model-based estimates and the one estimated using the nonlinear approach compared to the multilinear approach. The nonlinear approach relatively increases by 21%-23% the correlation coefficient and reduce RMSE by 0.007Wm^{-2} to 0.011 Wm^{-2} compared to multilinear approach. The nonlinear fitting approach reduces the relative difference by 36%-39% compare to the multilinear regression method. The RF_{aci} is found to be consistent with the value found by statistical relationship between aerosol and cloud properties from MODIS and CERES, respectively, and radiative transfer calculations. Further studies using the data retrieved from advanced instruments e.g. lidar and radar may be useful to test the assumption made in the present study concerning the proxy of aerosol column, the overestimation of AOD over land and deal with the multi-layer clouds.

Acknowledgments

The authors gratefully acknowledge the constant encouragement received from the Director, SAC for carrying out the present research work. Valuable suggestions received from Deputy Director, EPSA, and Head, CVD also gratefully acknowledged. CERES SSF data were obtained from the NASA Langley Research Centre Atmospheric Sciences Data Centre (ASDC), and MODIS data used in this study were acquired as part of NASA(tm)s Earth Science Enterprise. The MODIS Science Teams developed the algorithms for the AOD retrievals. The data were processed by the MODIS Adaptive Processing System for the AOD retrievals. The data were processed by the MODIS Adaptive Processing System and the Goddard Distributed Active Archive (DAAC). The Dutch-Finnish built OMI instrument is part of the NASA EOS Aura satellite payload. The OMI project is managed by NIVR and KNMI in Netherlands. The OMI data were also obtained from the DAAC. Reanalysis data are from the European Centre for Medium-Range Weather Forecasts. The authors would like to thank the data distribution centers for their support, Markand Oza for helpful discussion, and family for their continuous motivation. JQ acknowledges funding by the European Research Council (GA no 306284). The authors are grateful to two anonymous reviewers for constructive and useful comments.

References

Albrecht, B. A. (1989). Aerosols, cloud microphysics, and fractional cloudiness. Science, 245(4923), 1227–1230. doi:10.1126/science.245.4923.1227

Bellouin, N., Jones, A., Haywood, J., & Christopher, S. A. (2008). Updated estimate of aerosol direct Radiative forcing from satellite observations and comparison against the centre climate model. J. Geophys. Res. Atmos., 113(10). doi:10.1029/2007JD009385

Bellouin, N., Quaas, J., Morcrette, J. J., & Boucher, O. (2013). Estimates of aerosol radiative forcing from the MACC re-analysis. Atmos. Chem. Phys., 13(4), 2045–2062. doi:10.5194/acp-13-2045-2013

Bennartz, R. (2007) Global assessment of marine boundary layer cloud droplet number concentration from satellite. J. Geophys. Res., 112, 10.1029/2006jd007547.

Bennartz, R., and Rausch, J. (2017) "Global and regional estimates of warm cloud droplet number concentration based on 13 years of AQUA-MODIS observations. Atmos. Chem. Phys. Discuss., doi:10.5194/acp-2016-1130.

391 Brenguier, J.-L., Pawlowska, H., Schüller, L., Preusker, R., Fischer, J., & Fouquart, Y. (2000).
392 Radiative Properties of Boundary Layer Clouds: Droplet Effective Radius versus Number
393 Concentration. J. Atmos. Sci., 57(6), 803–821.
394 Boucher, O., Randall, D., Artaxo, P., Bretherton, C., Feingold, G., Forster, P., et al. (2013)
395 Clouds and aerosols. In: Stocker TF, Qin D, Plattner GK, Tignor M, Allen SK, Boschung J,
396 et al., editors. Climate change 2013: the physical science basis. Contribution of Working
397 Group I to the Fifth Assessment Report of the Intergovernmental Panel on Climate Change.
398 Cambridge, UK, and New York, NY, USA: Cambridge University Press; pp. 571 – 658.
399 Cherian, R., Venkataraman, C., Quaas, J., Ramachandran, S. (2013). GCM simulations of
400 anthropgenic aerosol-induced cahnges in aerosol extinction, atmiospheric heating and
401 precepitaion over India. J. Geophys. Res. Atmos, 11:2938–2955. doi:10.1002/jgrd.50298
402 Chin, M., Rood, R.B., Lin, S.J., Muller, J.F., Thompson, A.M., 2000. Atmospheric sulfur cycle
403 simulated in the global model GOCART: model description and global properties. J.
404 Geophys. Res. 105, 24,671-24,687.
405 Das, S., Dey, S., and Dash, S. K. (2015). Direct radiative effects of anthropogenic aerosols on
406 Indian summer monsoon circulation. Theor. Appl. Climatol., doi: 10.1007/s00704-015-
407 1444-8
408 Feingold, G., Remer, L. A., Ramaprasad, J., and Kaufman, Y. J. (2001). Analysis of smoke
409 impact on clouds in Brazilian biomass burning regions: An extension of Twomey's
410 approach. J. Geophys. Res., 106, 22907–22922.
411 Feingold, G., Eberhard, W. L., Veron, D. E., and Previdi, M. (2003). First measurements of the
412 Twomey indirect e ff ect using ground-based remote sensors, Geophys. Res. Lett., 30, 1287,
413 doi:10.1029/2002GL016633.
414 Girolamo, L.D., Bond, T.C., Bramer, D., Diner, D.J., Fettinger, F., Kahn, R.A., Martonchik,
415 J.V., Ramana, M.V., Ramanathan, V., Rasch, P.J., 2004. Analysis of Multi-angle Imaging
416 Spectroradiometer (MISR) aerosol optical depths over greater India during winter 2001 e
417 2004. Geophys. Res. Lett., 31, L23115. http://dx.doi.org/10.1029/2004GL021273.
418 Huber, M., & Knutti, R. (2011). Anthropogenic and natural warming inferred from changes in
419 Earth's energy balance. Nat. Geosci., doi:10.1038/ngeo1327
420 Intergovernmental Panel on Climate Change (IPCC) (2007), Climate Change 2007: The
421 Physical Scientific Basis, edited by S. Solomon et al., Cambridge Univ. Press, New York.
422 Kim, J., Lee, J., Lee, H. C., Higurashi, A., Takemura, T., & Song, C. H. (2007). Consistency
423 of the aerosol type classification from satellite remote sensing during the Atmospheric
424 Brown Cloud-East Asia Regional Experiment campaign. J. Geophys. Res. Atmos., 112(22).
425 doi:10.1029/2006JD008201
426 Koren, I., Remer, L. A., Kaufman, Y. J., Rudich, Y., & Martins, J. V. (2007). On the twilight
427 zone between clouds and aerosols. Geophys. Res. Lett., 34(8). doi:10.1029/2007GL029253
428 Levelt, P. F., Van Den Oord, G. H. J., Dobber, M. R., Mälkki, A., Visser, H., De Vries, J., …
429 Saari, H. (2006). The ozone monitoring instrument. IEEE Trans. Geosci. Remote Sens.,
430 44(5), 1093–1100. doi:10.1109/TGRS.2006.872333
431 Levenberg, K. (1944). A Method for the Solution of Certain Non-Linear Problems in Least
432 Squares, Q. Appl. Math., 2,164-168.
433 Levy, R. C., Remer, L. A., Mattoo, S., Vermote, E. F., & Kaufman, Y. J. (2007). Second-
434 generation operational algorithm: Retrieval of aerosol properties over land from inversion
435 of Moderate Resolution Imaging Spectroradiometer spectral reflectance. J. Geophys. Res.
436 Atmos., 112(13). doi:10.1029/2006JD007811
437 Liu, J., Mauzerall, D.L., Horowitz, L.W., 2009. Evaluating inter-continental transport of fine
438 aerosols: (2) global health impact. Atmos. Environ. 43, 4339-4347.
439 Loeb, N.: Angular models: Instantaneous and ensemble accuracy, in: 1st CERES-II Science
440 Team Meeting Proceedings, NCAR, Boulder, Colorado, USA, 2004.

441 Loeb, N. G., B. A. Wielicki, W. Su, K. Loukachine, W. Sun, T. Wong, K. J. Priestley, G.
442 Matthews, W. F. Miller, and R. Davies (2007), Multi-instrument comparison of top-of-
443 atmosphere reflected solar radiation, J. Clim., 20, 575–591.
444 Ma, X., Fangqun, Yu., and Quaas, J., (2014). Reassessment of satellite-based estimate of
445 aerosol cloud forcing. J. Geophys. Res. Atmos., 119, 10,394-10,409,
446 doi:10.1002/2014JD021670.
447 McComiskey, A., Feingold, G., Frisch, A. S., Turner, D. D., Miller, M. A., Chiu, J. C., Min,
448 Q., and Ogren, J. A. (2009). An assessment of aerosol-cloud interactions in marine stratus
449 clouds based on surface remote sensing. J. Geophys. Res., 114, D09203,
450 doi:10.1029/2008JD011006.
451 McComiskey, A., Feingold, G. (2012). The scale problem in quantifying aerosol indirect
452 effects. Atmos. Chem. Phys., 12(2), 1031–1049.
453 Minnis, P., D. F. Young, S. Sun-Mack, P. W. Heck, D. R. Doelling, and Q. Z. Trepte (2003),
454 CERES cloud property retrievals from imagers on TRMM, Terra, and Aqua, in Proc. SPIE
455 10th International Symposium on Remote Sensing: Conference on Remote Sensing of
456 Clouds and the Atmosphere VII, vol. 5235, pp. 37–48, Barcelona, Spain.
457 Minnis, P., D. F. Young, S. Sun-Mack, Q. Trepte, D. R. Doelling, D. A. Spangenberg, and P.
458 W. Heck (2004), Ceres cloud products, in 1st CERES-II Science Team Meeting
459 Proceedings, NCAR, Boulder, Colorado.
460 Moorthy, K.K., Babu, S.S., Manoj, M.R., Satheesh, S.K., 2013. Buildup of aerosols over the
461 Indian region. Geophys. Res. Lett. 40, 1011-1014.
462 http://dx.doi.org/10.1029/2012GL054876.
463 Moorthy, K.K., et al. (2015). South Asian aerosols in perspective: Preface to the special issue.
464 Atmos. Environ., http://dx.doi.org/10.1016/j.atmosenv.2015.10.073.
465 Parkinson, C. L. (2003). Aqua: An earth-observing satellite mission to examine water and other
466 climate variables. IEEE Trans. Geosci. Remote Sens., 41, 173–183.
467 doi:10.1109/TGRS.2002.808319
468 Penner, J. E., Xu, L., & Wang, M. (2011). Satellite methods underestimate indirect climate
469 forcing by aerosols. Proc. Natl. Acad. Sci. U.S.A., 108(33), 13404–13408.
470 doi:10.1073/pnas.1018526108
471 Penner, J. E., Zhou, C., & Xu, L. (2012). Consistent estimates from satellites and models for
472 the first aerosol indirect forcing. Geophys. Res. Lett., 39(13). doi:10.1029/2012GL051870
473 Quaas, J., Boucher, O., Bellouin, N., & Kinne, S. (2008). Satellite-based estimate of the direct
474 and indirect aerosol climate forcing. J. Geophys. Res. Atmos., 113(5), 1–9.
475 doi:10.1029/2007JD008962
476 Quaas, J., Boucher, O., & Bréon, F. M. (2004). Aerosol indirect effects in POLDER satellite
477 data and the Laboratoire de Météorologie Dynamique-Zoom (LMDZ) general circulation
478 model. J. Geophys. Res. Atmos., 109(8). doi:10.1029/2003JD004317
479 Quaas, J., O. Boucher, and U. Lohmann (2006), Constraining the total aerosol indirect effect
480 in the LMDZ and ECHAM4 GCMs using MODIS satellite data, Atmos. Chem. Phys., 6,
481 947– 955.
482 Quaas, J., Ming, Y., Menon, S., Takemura, T., Wang, M., Penner, J. E., … Schulz, M. (2009).
483 Aerosol indirect effects – general circulation model intercomparison and evaluation with
484 satellite data. Atmos. Chem. Phys., 9(22), 8697–8717. doi:10.5194/acp-9-8697-2009
485 Quaas, J., O. Boucher, N. Bellouin, and S. Kinne (2011), Which of satellite- or model-based
486 estimates is closer to reality for aerosol indirect forcing?, Proc. Natl. Acad. Sci. U.S.A., 108,
487 E1099.
488 Rausch, J., Heidinger, A., and Bennartz, R. (2010). Regional assessment of microphysical
489 properties of marine boundary layer cloud using the PATMOS-x dataset, J. Geophys. Res.
490 Atmos., 115, 10.1029/2010jd014468.

Remer, L. A., Kaufman, Y. J., Tanré, D., Mattoo, S., Chu, D. A., Martins, J. V., … Holben, B. N. (2005). The MODIS Aerosol Algorithm, Products, and Validation. J. Atmos. Sci., 62(4), 947–973. doi:10.1175/JAS3385.1

Ricchiazzi, P., Yang, S., Gautier, C., & Sowle, D. (1998). SBDART: A Research and Teaching Software Tool for Plane-Parallel Radiative Transfer in the Earth's Atmosphere. B. Am. Meteorol. Soc., 79(10), 2101–2114.

Schoeberl, M. R., Douglass, A. R., Hilsenrath, E., Bhartia, P. K., Beer, R., Waters, J. W., … DeCola, P. (2006). Overview of the EOS aura mission. IEEE Trans. Geosci. Remote Sens., 44(5), 1066–1072. doi: 10.1109/TGRS.2005.861950

Schüller, L., R. Bennartz, J. Fischer, and J.-L. Brenguier (2005), An algorithm for the retrieval of droplet number concentration and geometrical thickness of stratiform marine boundary layer clouds applied to MODIS radiometric observations, J. Appl. Meteorol., 44, 28– 38.

Stamnes, K., Tsay, S. C., Wiscombe, W., & Jayaweera, K. (1988). Numerically stable algorithm for discrete-ordinate-method radiative transfer in multiple scattering and emitting layered media. Appl. Optics, 27(12), 2502–2509. doi:10.1364/AO.27.002502

Tiwari, S., Mishra, A. K., and Singh, A K. (2015). Aerosol climatology over the Bay of Bengal and Arabian Sea inferred from sapce-borne radiometers and lidar observations. Aerosol Air Qual. Res., doi:10.4209/aaqr.2015.06.0406.

Torres, O., Bhartia, P. K., Herman, J. R., Ahmad, Z., & Gleason, J. (1998). Derivation of aerosol properties from satellite measurements of backscattered ultraviolet radiation: Theoretical basis. J. Geophys. Res. Atmos., 103(D14), 17099–17110. doi: 10.1029/98JD00900

Transtrum, M. K., Machta, B. B., and Sethna, J.P. (2010). Why are nonlinear fits to data so challenging? Phys. Rev. Lett. 104, 060201.

Transtrum, M. K., and Sethna, J.P. (2012). Improvements to the Levenberg-Marquardt algorithm for nonlinear least-squares minimization. J. Comput. Phys., https://arXiv.org/abs/1201.5885v1.

Twomey, S. (1977). The Influence of Pollution on the Shortwave Albedo of Clouds. J. Atmos. Sci..

Wen, G., Marshak, A., Cahalan, R. F., Remer, L. A., & Kleidman, R. G. (2007). 3-D aerosol-cloud radiative interaction observed in collocated MODIS and ASTER images of cumulus cloud fields. J. Geophys. Res. Atmos., 112(13). doi:10.1029/2006JD008267

Wielicki, B. A., Barkstrom, B. R., Harrison, E. F., Lee, R. B., Smith, G. L., & Cooper, J. E. (1996). Clouds and the Earth's Radiant Energy System (CERES): An Earth Observing System Experiment. B. Am. Meteorol. Soc., 77(5), 853–868.

528

529

530 **Table 1**: The list of parameters and their sources used as an input to the SDBART model for
531 the simulation of RF_{aci}.
532

Input parameters	Source
Temperature and Water vapor (for 32 layers extending from 1000 to 1 hPa)	ECMWF reanalysis
Total Columnar ozone	OMI-AURA
Surface Albedo	For land - 0.15 For ocean - default value of "ocean" (given in SBDART)
cloud effective droplet radius cloud liquid water path cloud fraction	MODIS retrievals reported in CERES-SSF product
geometrical thickness of cloud	Computed from MODIS and ECMWF data

533

534

535

536 **Table 2:** Seasonal and regional sensitivities d ln N_d/d ln τ_a of cloud droplet number
537 concentration N_d to changes in aerosol optical depth used in this study. The given standard
538 deviation is derived from minimum and maximum values for a particular season. The
539 associated range in RF_{aci} is also estimated where the standard deviation of RF_{aci} shows the
540 variation due to change in d ln Nd / d ln τ_a.

	Region	Winter	Pre-Monsoon	Monsoon	Post-Monsoon
$\frac{d \ln N_d}{d \ln \tau}$	AS	0.384 ± 0.146	0.408 ± 0.189	0.272 ± 0.131	0.18 ± 0.102
	BOB	0.314 ± 0.136	0.414 ± 0.15	0.194 ± 0.104	0.148 ± 0.088
	CI	0.214 ± 0.107	0.178 ± 0.105	0.107 ± 0.069	0.122 ± 0.071
Rf_{aci} for Anthrophonic Fraction	AS	-0.19 ± 0.036	-0.14 ± 0.056	-0.08 ± 0.036	-0.16 ± 0.036
	BOB	-0.22 ± 0.062	-0.16 ± 0.036	-0.07 ± 0.02	-0.2 ± 0.036
	CI	-0.13 ± 0.02	-0.2 ± 0.036	-0.05 ± 0.034	-0.16 ± 0.036
Rf_{aci} for Natural Fraction	AS	-0.12 ± 0.036	-0.18 ± 0.036	-0.03 ± 0.04	-0.06 ± 0.036
	BOB	-0.08 ± 0.026	-0.11 ± 0.026	-0.04 ± 0.039	-0.06 ± 0.017
	CI	-0.16 ± 0.027	-0.22 ± 0.055	-0.1 ± 0.027	-0.14 ± 0.036

541

542

Table 3: Lists the sources of uncertainties and their values involved in the satellite-based estimate of RF_{aci} in the present study.

Source of uncertainty	Values
Total AOD	$0.03 \pm 0.05.\tau_a$ over ocean $0.05 \pm 0.05.\tau_a$ over land
MODIS-OMI algorithm (for the estimate of anthropogenic and natural fraction of aerosol)	1σ standard deviation as per below table-S2
Flux retrieval from CERES	5%
Cloud optical depth retrieval from CERES	21%
Cloud droplet number concentration	See table-2
Statistical fitting approach	0.021 W m^{-2} in nonlinear for anthropogenic 0.032 W m^{-2} in nonlinear for natural 0.033 W m^{-2} in multilinear for anthropogenic 0.053 W m^{-2} in multilinear for natural

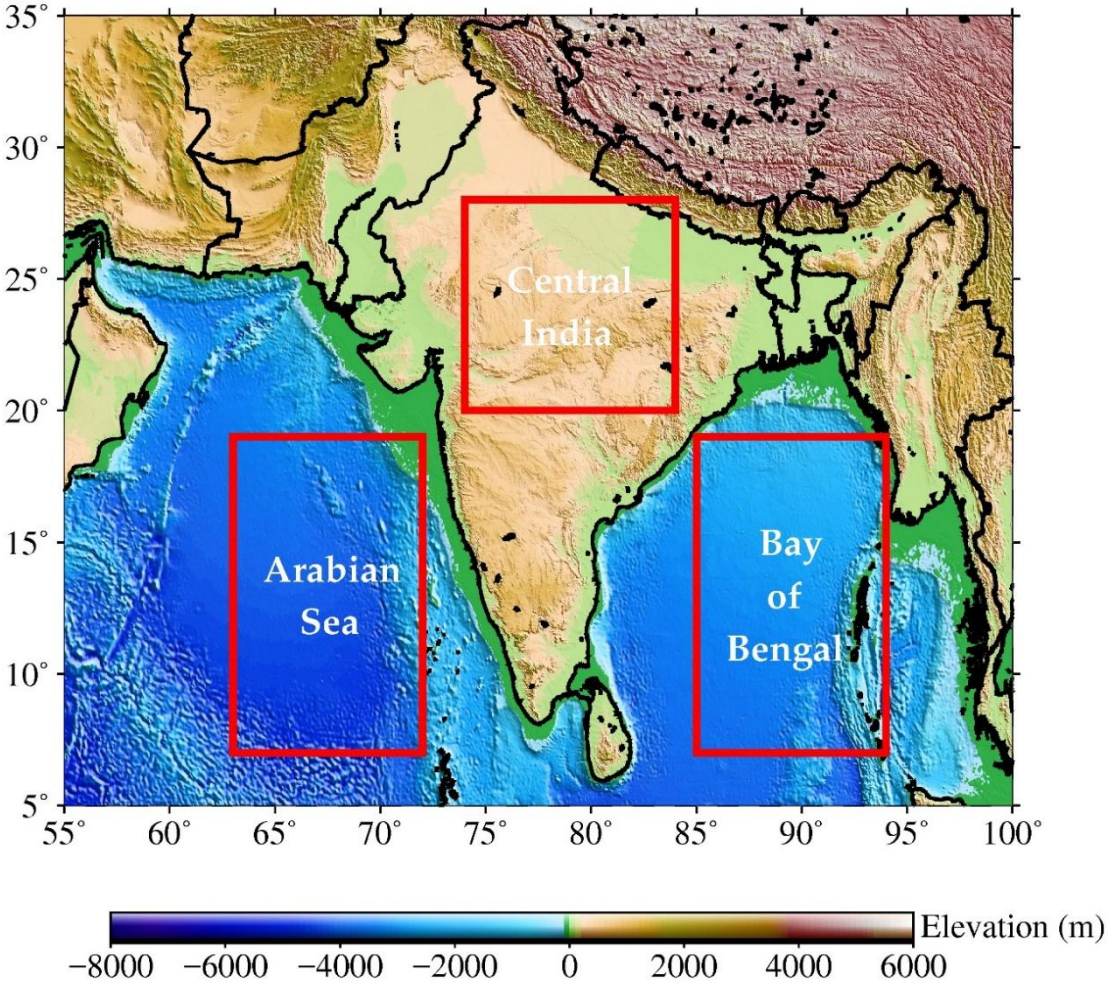

Figure 1: Map of India and surroundings showing the study regions. The regions covered by red box represent the study locations (Arabian Sea, Bay of Bengal and Central India).

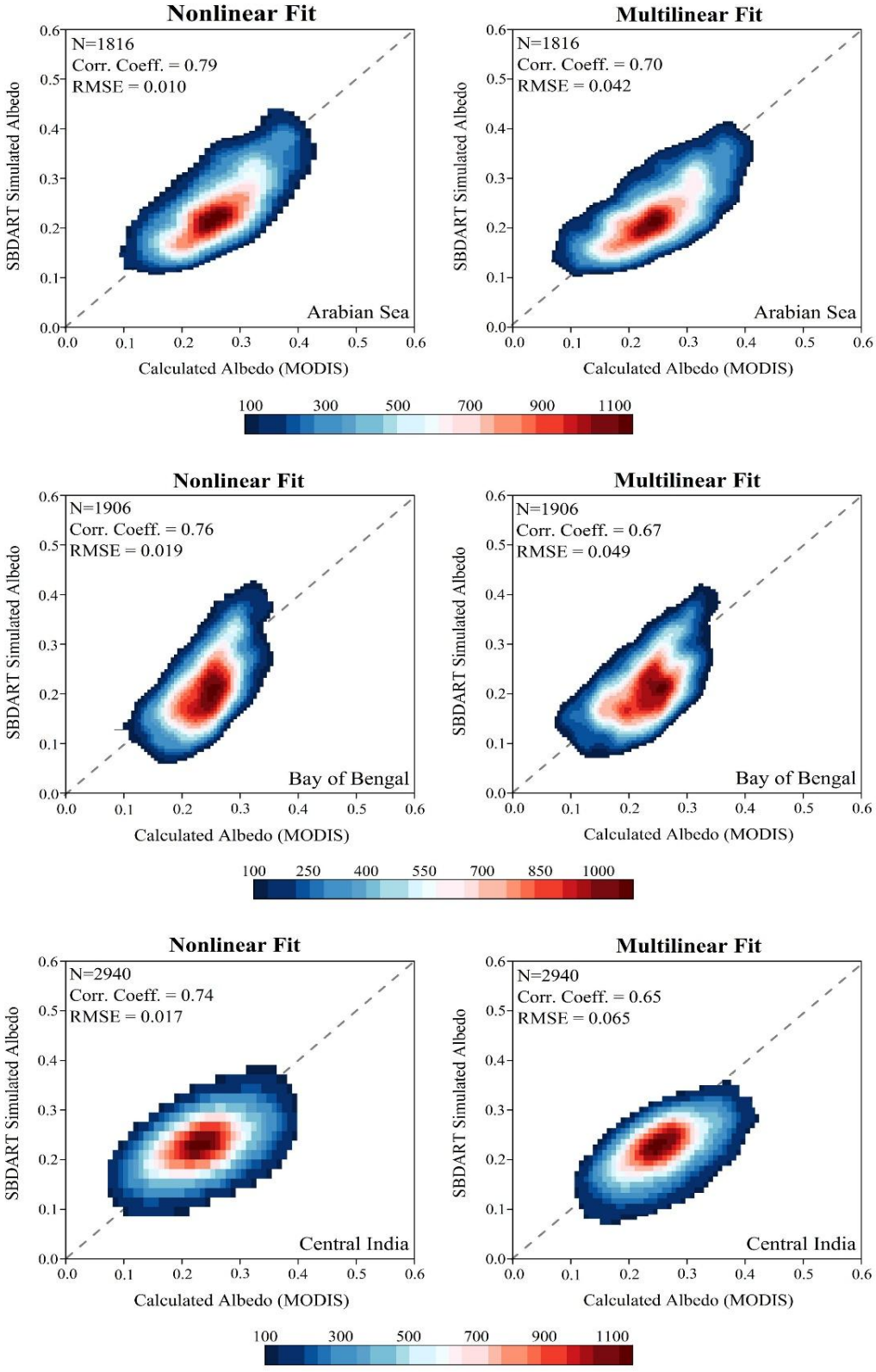

Figure 2: Scatter density plots of model-simulated albedo and the one computed using both statistical fitting method (nonlinear and multilinear fit) using satellite measurements for all three regions.

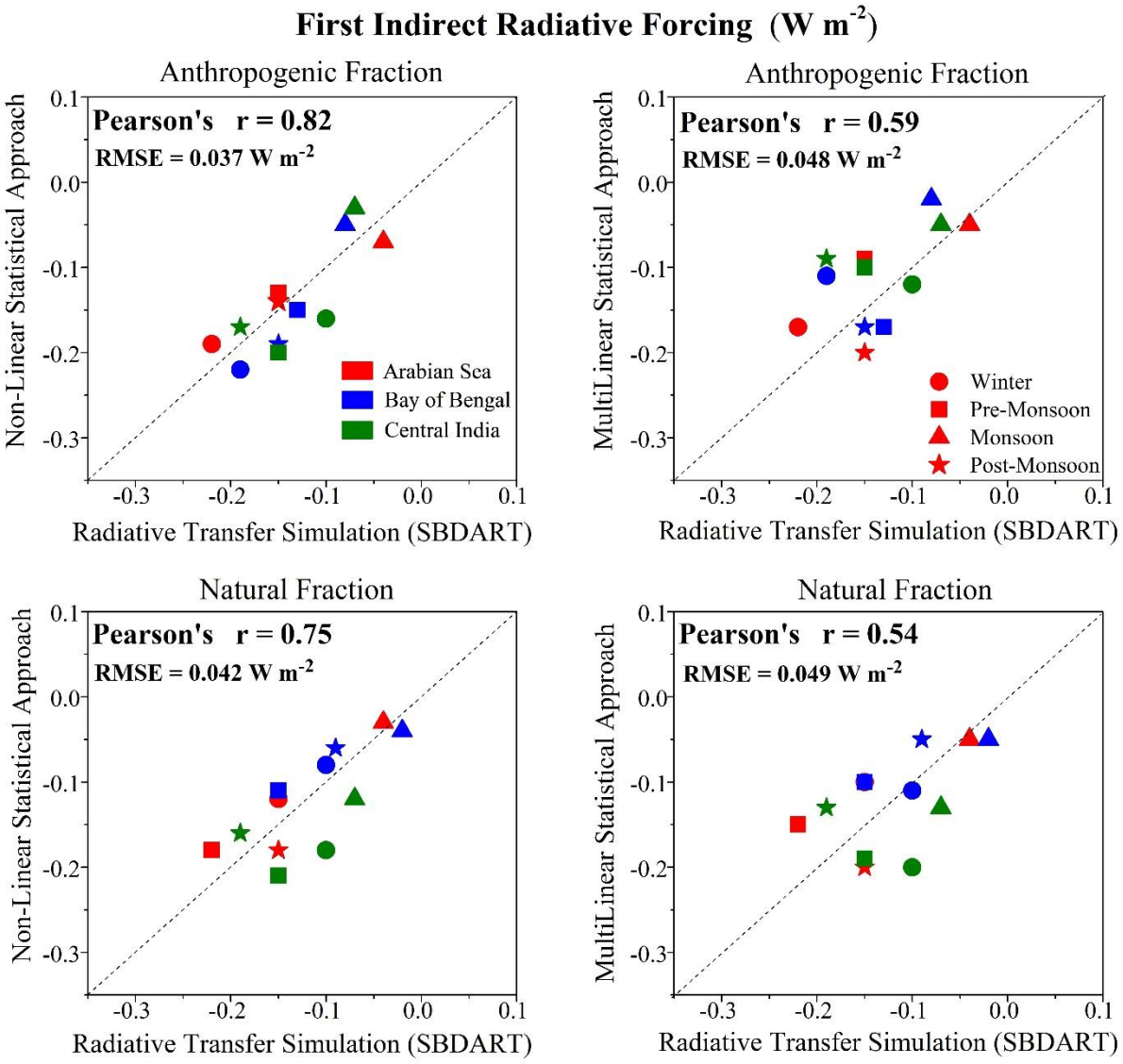

Figure 3: Comparison between satellite-based RFaci using both statistical fits and the one simulated by the SBDART model for all three regions and for all seasons. The different color indicates the regions, whereas the different symbols indicates the different seasons. Note that the fit is separately performed for each season and each region.

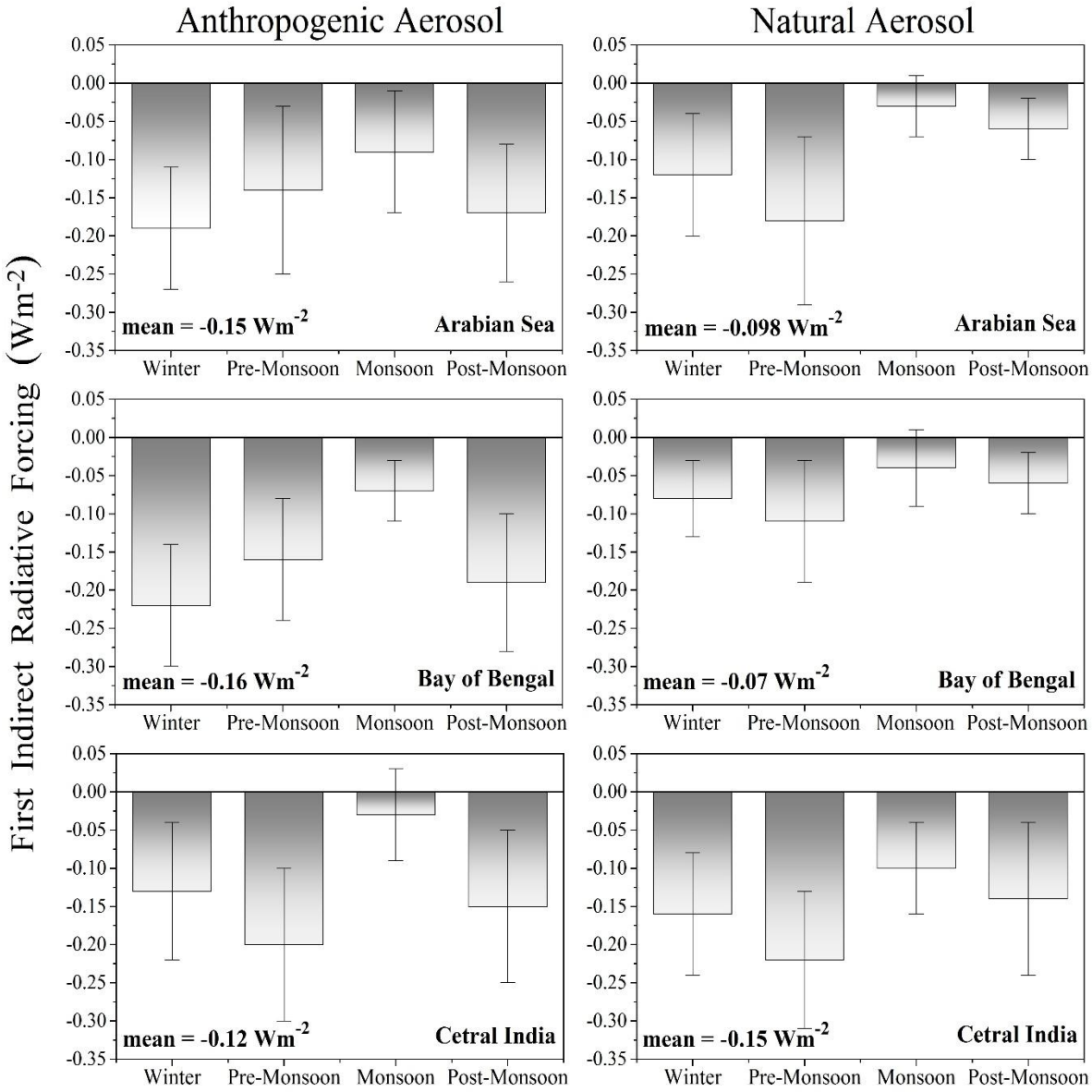

Figure 4: Seasonal variability of six-year averaged RFaci obtained using the nonlinear fit for all three regions for both anthropogenic and natural aerosols along with mean values.